Activation Energy Paths for Graphene Nucleation and Growth on Cu

HoKwon Kim,[†] Cecilia Mattevi,[*,†] M. Reyes Calvo,[‡] Jenny C. Oberg,[‡,§] Luca Artiglia,[⊥] Stefano Agnoli,[⊥] Cyrus F. Hirjibehedin,[‡,§,¶] Manish Chhowalla,[#] and Eduardo Saiz[†]

[†]CASC, Department of Materials, Imperial College London, London SW7 2AZ, U.K., [‡]London Centre for Nanotechnology, University College London, London WC1H 0AH, U.K., [§]Department of Physics & Astronomy, University College London, London WC1E 6BT, U.K., [⊥]Department of Chemical Science, University of Padova, Padova, I-35131, Italy, [¶]Department of Chemistry, University College London, London WC1H 0AJ, U.K., and [#]Materials Science and Engineering, Rutgers University, Piscataway, New Jersey 08854, United States

ABSTRACT

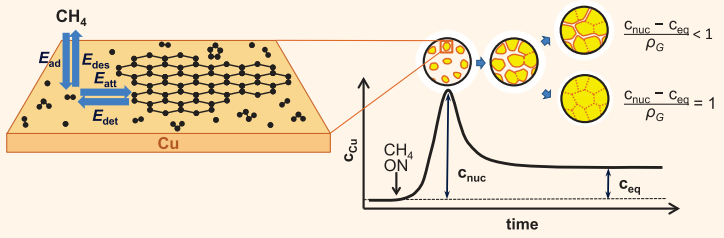

The synthesis of wafer-scale single crystal graphene remains a challenge toward the utilization of its intrinsic properties in electronics. Until now, the large-area chemical vapor deposition of graphene has yielded a polycrystalline material, where grain boundaries are detrimental to its electrical properties. Here, we study the physicochemical mechanisms underlying the nucleation and growth kinetics of graphene on copper, providing new insights necessary for the engineering synthesis of wafer-scale single crystals. Graphene arises from the crystallization of a supersaturated fraction of carbon-adatom species, and its nucleation density is the result of competition between the mobility of the carbon-adatom species and their desorption rate. As the energetics of these phenomena varies with temperature, the nucleation activation energies can span over a wide range (1−3 eV) leading to a rational prediction of the individual nuclei size and density distribution. The growth-limiting step was found to be the attachment of carbon-adatom species to the graphene edges, which was independent of the Cu crystalline orientation.

KEYWORDS: chemical vapor deposition · graphene · nucleation and growth · surface catalysis · 2D nanomaterial · large-area optoelectronics

Chemical vapor deposition (CVD) of graphene on copper[1] has enabled the growth of single layer graphene over large areas and its implementation into electronics. However, CVD graphene is defective as compared to mechanically exfoliated graphene[2,3] because its polycrystalline nature results in grain boundaries that are responsible for diminished electrical and mechanical properties. Only a wafer-scale single crystal graphene can yield the benefits of its intrinsic properties. To this end, although much effort has been placed on the improvement of CVD graphene, most of the advances have been achieved primarily through empirical optimization of the growth parameters.[4−7] A full understanding of the precise physicochemical mechanisms that govern film formation and that can potentially lead to the rational engineering of the growth of wafer-scale single crystal graphene is still lacking. The challenge is to link atomic level phenomena such as adsorption, diffusion, and nucleation with nano- to microscale features like substrate roughness, crystallinity, and grain boundaries.

Here, we focus on the formation of graphene on Cu. We systematically analyze the CVD process in the framework of existing theories for two-dimensional nucleation and growth of thin films, which describe the key stages that determine the nucleation density, distribution of nuclei, and final coverage. We have identified competing atomic phenomena such as adatom mobility versus desorption whose balance defines characteristic nucleation regimes with very different activation energies depending on the temperature. The growth rates are limited by carbon attachment to the graphene edges without significant dependence on the crystal orientation of the Cu substrate. However, both nucleation and growth are affected by the microscopic substrate roughness that determines nuclei distribution and can impart distinctive morphological features to the final film. Predicting whether a given growth condition would produce a continuous, pinhole-free graphene film is possible by knowing the difference between the supersaturation carbon concentration, which is needed to nucleate graphene, and the equilibrium concentration of carbon adsorbed species on the Cu surface. Our study offers new fundamental insights on the CVD graphene

* Address correspondence to c.mattevi@imperial.ac.uk.

Received for review February 28, 2012 and accepted March 25, 2012.

Published online March 25, 2012
10.1021/nn3008965

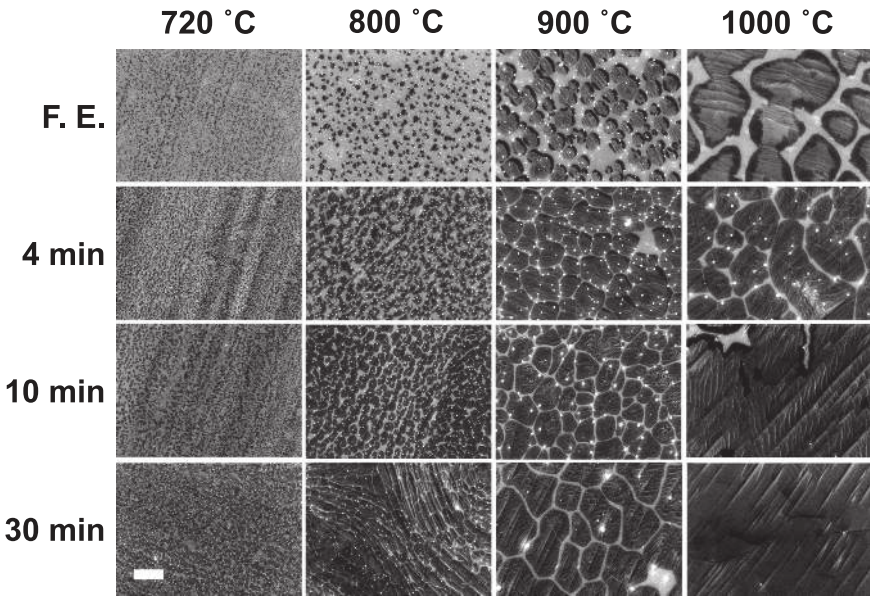

Figure 1. High-resolution scanning electron microscope (SEM) images of graphene nuclei grown on Cu for different growth temperatures and times. These are identifiable as areas darker than the exposed Cu surface, which quickly oxidize in air after being taken out from the CVD growth system. Scale bar: 1 μm.

growth, highlighting the key distinguishing aspects and defining clear guidelines for the large-scale fabrication of high quality graphene and ultimately, single crystal graphene films.

RESULTS AND DISCUSSION

We investigated the growth of graphene from 720 °C up to 1050 °C (Methods section and Supporting Information, Figure S1) for different time lengths, from a flash exposure to methane up to 30 min in order to follow the evolution of the graphene and to extract the growth rates. The temperature range of growth includes the minimum temperature (720 °C) at which graphene nucleation was observed while the maximum temperature (1050 °C) was chosen close to the Cu melting point (1084 °C). To understand the effect of substrate on graphene formation, we carefully characterized crystallinity and morphology of the Cu substrates before and after annealing at the growth temperatures as reported in the Supporting Information, Figure S1. Upon exposure to CH_4, graphene nucleates very rapidly, grows, and coalesces to form large domains (Figure 1). With the use of this growth approach, three key phenomena attracted our attention: (1) nucleation only occurs during the initial instants and no new nuclei are formed even after only 4 min of growth time at any temperature (Figure 1); (2) higher temperature leads to a lower density of nuclei with larger lateral size (Figure 1 and 2a); (3) the domains do not evolve to fully cover the substrate surface, rather, the fractional coverage of graphene saturates for temperatures below 1000 °C, under our experimental conditions. Growth times as long as up to 150 min have been attempted, but the area of graphene never reached a complete surface coverage with pores remaining in the film. To obtain a continuous graphene film we needed to reach growth temperature of $\cong$1000 °C and exposure time of about 30 min. This continuous film is mostly a single graphene layer as Raman spectroscopy and scanning tunneling microscope (STM) indicate (Figure 2 panels b and c, respectively). The 2D/G peak ratio is about 2 and the 2D fwhm is about 28 cm^{-1} as reported for single layer graphene grown by CVD.[1] In addition, the D peak is negligible over most of the surface scanned, suggesting reasonably good continuity of the film and a low level of defects. The STM image shows the expected linear Moiré pattern generated by the presence of a Cu lattice with (100) crystallographic orientation.[8] It is worth noting that the individual flow rates of H_2 and CH_4 and the growth pressure of the CVD process were chosen so that growth occurs in the surface reaction regime[7] to obtain single layer of graphene over more than 95% of the surface. These conditions were kept constant throughout the study unless otherwise noted.

The kinetics of two-dimensional nucleation and growth on surfaces has been both theoretically and experimentally investigated extensively in other systems, for example, thin film deposition and crystallization of amorphous phases at surfaces. We employ a general approach based on the ubiquitous model developed by Robinson and Robins[9] on the nucleation of metal thin films on ceramic substrates and the Johnson–Mehl–Avrami–Kolmogorov (JMAK) model of phase transformation[10–12] to understand from an atomistic to macroscopic level the nucleation and growth of graphene on a Cu surface.

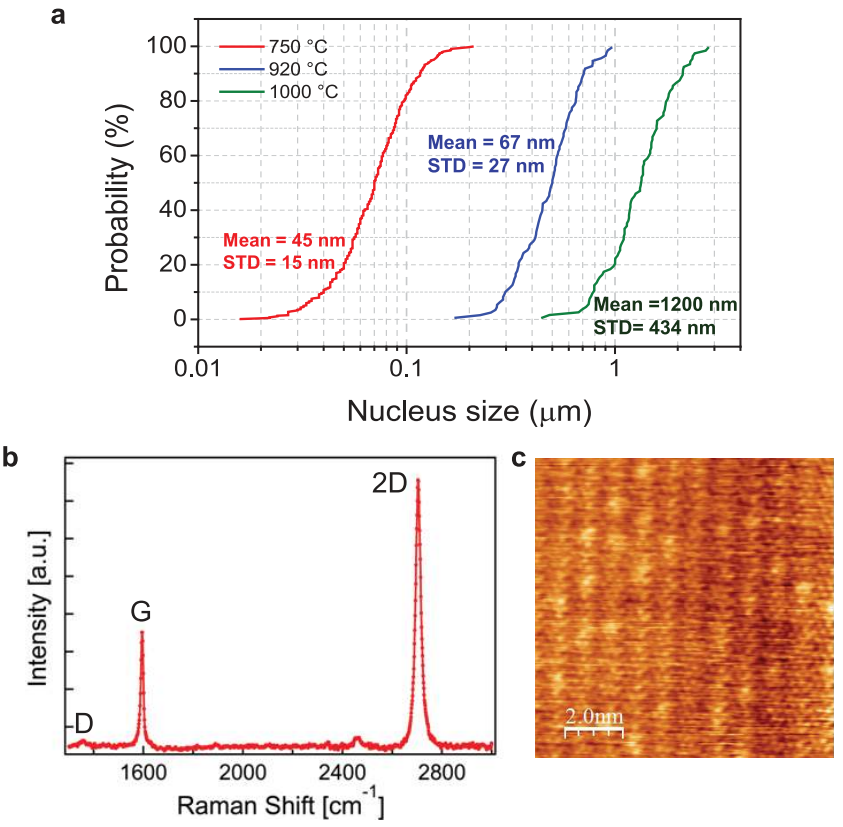

Figure 2. Graphene thin film characteristics. (a) Cumulative distribution plot of graphene nucleus size of graphene/Cu samples obtained at flash exposure for growth temperatures, 750 °C, 920 °C, and 1000 °C. The probability has been calculated based on the graphene nucleus size measurements on the large area SEM images from respective conditions. (b) Raman spectra and (c) atomic scale STM image recorded with an Omicron LT-STM at 77 K of a continuous monolayer graphene film grown at 1000 °C. The relatively low D peak and the ordered lattice structure demonstrate the high crystal quality of the film.

Figure 3 illustrates the overall processes of graphene formation on Cu on the bases of the models developed for graphene growth on metals with higher carbon affinity (namely with higher carbon solubility).[13,14] Upon the breakdown of methane through dissociative chemisorption on the Cu surface, the concentration of the active carbon species, c_{cu}, increases until it reaches a critical supersaturation level (c_{nuc}), where nucleation of stable graphene nuclei takes place. As the nucleation and growth of the supercritical nuclei deplete the adsorbed carbon species surrounding them, the c_{cu} is quickly reduced to a level where the nucleation rate is negligible while growth of the nuclei continues until the supersaturated amount of surface carbon species above the equilibrium level c_{eq} is consumed and the equilibrium between graphene, surface carbon, and CH_4/H_2 is reached. Depending on the available carbon, the degree of supersaturation ($c_{nuc} - c_{eq}$), graphene nuclei either coalesce to form eventually a continuous film or stop growing to reach a saturated, final incomplete coverage.[13,14]

It must be noted that the exact nature of the active carbon species adsorbed on the Cu surface that leads to graphene nucleation has not been well identified yet. Several theoretical calculations[15−17] have predicted that the dissociation of methane to a carbon monomer on Cu is highly endothermic and carbon dimers are more stable than isolated C adatoms (by over 2 eV) as the carbon−Cu interaction is weak and the diffusion barrier of carbon is low. In the surface mediated growth of graphene on Ru, Ir, 5-atom carbon clusters were found to be direct precursors of a stable nucleus.[14,15] However, here, we generally refer to the active carbon species as carbon monomers because there is no conclusive experimental evidence for the presence of carbon aggregates based on our analysis. However, additional work is necessary to definitively rule out the absence of aggregates. We also rule out that high temperature poisoning by noncarbon impurities at the surface could be the reason for the observed growth saturation behavior on the bases of X-ray photoelectron spectroscopy (XPS) characterizations (Supporting Information, Figure S3).

To understand the nucleation kinetics within the framework of the existing nucleation model, we need to examine the density of nuclei as a function of temperature. Figure 4a shows the Arrhenius plot of the temperature dependent density of graphene nuclei estimated from the density of graphene nuclei at flash exposure. We could identify two distinct slopes

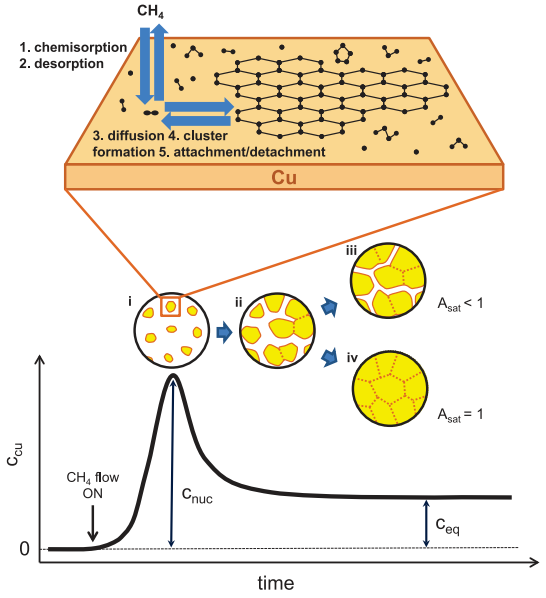

Figure 3. Overall illustration of the nucleation and growth mechanism of graphene on Cu. The decomposition of methane leads to supersaturation of carbon adatoms at the Cu surface. When c_{cu} reaches a critical supersaturation point (c_{nuc}) graphene domains nucleate and begin to grow, possibly involving multiatom carbon cluster formation and attachment of the clusters (i). Graphene nuclei coalesce as the growth proceeds further (ii). The growth stops either when the amount of superstaurated carbon species are consumed (iii) or when the domains merge together to completely cover the surface of Cu (iv).

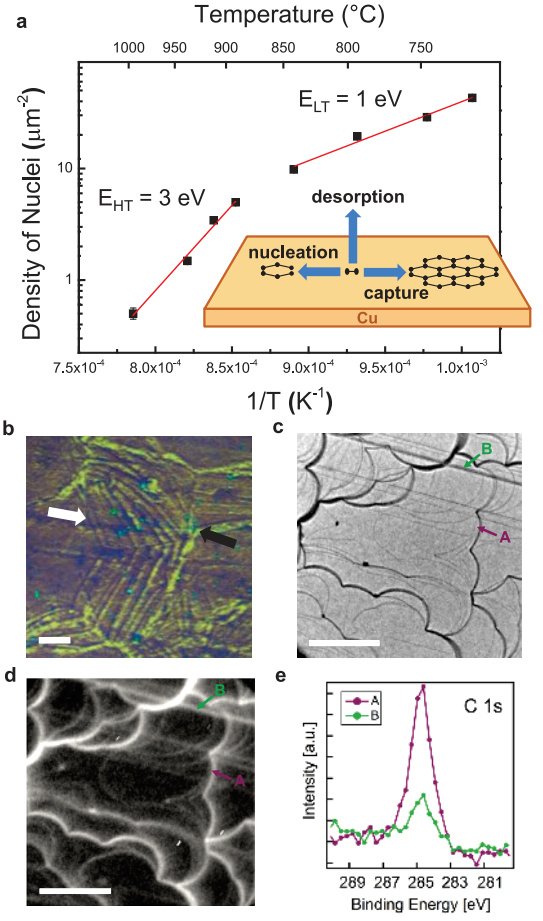

Figure 4. Analysis of graphene nucleation behavior. (a) Natural logarithm of density of graphene nuclei *vs* 1/*T* from SEM analysis at flash exposure. The linear fits are performed for the two regimes; desorption controlled (>850 °C) and capture controlled (<850 °C). (b) Optical micrograph of transferred graphene onto SiO_2 where graphene thickness distribution reflects the Cu morphology. The darker multilayer regions (*e.g.*, white arrow) follow the grain boundaries and grooves of Cu underneath whereas brighter monolayer regions (*e.g.*, black arrow) appear on a smooth Cu surface. Scale bar: 10 μm. (c) The LEEM image (electron energy 3.5 eV) shows Cu (100) single crystal after several cycles of sputtering and annealing at 950 °C. Step edges (A) as well as dislocations (B) appear darker because of the different orientation with respect to the incident beam. Scale bar: 2 μm. (d) C1s XPEEM map of the same region in panel c demonstrates that carbon is preferentially segregated at the step edges (A) and at the dislocations (B) (photon energy = 397.05 eV). Scale bar: 2 μm. (e) C 1s spectra at the step edge (A) and dislocation (B) in the region marked in panels c and d.

(below and above 870 °C), which reflect the presence of two different nucleation mechanisms governed by different activation energies.

According to the Robinson and Robins model, under the assumption of temperature independent critical nucleus size, the occurrence of two nucleation regimes is a result of the competition between the processes of adatom capture, surface diffusion, and re-evaporation.[9,14,18] In the low temperature regime (<870 °C), the desorption of carbon adatoms is negligible due to its high activation energy (~ 6 eV)[16] so that the lifetime of an adatom at the surface before nucleation or attachment of carbon at the graphene nuclei edges is determined by carbon surface mobility. This regime then can be assigned as the capture controlled regime where the nucleation rate is limited by capture of a carbon adatoms by supercritical nucleus. In the high temperature regime (>870 °C), the desorption rate is significant compared to the mobility of carbon adatoms, so that the adatom lifetime and nucleation rate can be said to be desorption controlled.

The saturation density of nuclei (N_s) in the capture-controlled regime follows the following relationship under the assumption of atomic size critical nuclei for the methane partial pressure of P_{CH_4}:

$$N_s^3 \sim P_{CH_4} \times \exp\left(\frac{2E_{att} - E_d - E_{ad}}{kT}\right) \quad (1)$$

Therefore, the apparent nucleation activation energy in the low temperature regime corresponds to $E_{LT} = (2E_{att} - E_d - E_{ad})/3 = 1$ eV (Figure 4a), where E_{att} is a barrier of attachment for the capture of a monomer by supercritical nucleus, E_d is the activation energy of surface diffusion of a monomer, and E_{ad} is the activation energy for dissociative adsorption of CH_4 on Cu.

Similarly, in the desorption controlled regime,

$$N_s^2 \sim P_{CH_4} \times \exp\left(\frac{E_{des} + E_{att} - E_d - E_{ad}}{kT}\right) \quad (2)$$

the high temperature nucleation activation energy, $E_{HT} = (E_{des} + E_{att} - E_d - E_{ad})/2 = 3$ eV (Figure 4a) where

E_{des} is the desorption energy of a carbon monomer on the Cu surface.

Considering the known values of $E_d \approx 0.7-0.06$ eV,[17,19] $E_{ad} \approx 1.7-1.9$ eV,[20−22] $E_{des} \approx 6$ eV[16] on Cu and $E_{att} \approx 2$ eV estimated from the growth on Ru,[13] the obtained values of E_{LT} and E_{HT} are in reasonable agreement with the values expected from the model of capture-controlled and desorption controlled nucleation, respectively.

In both cases, the decrease in the saturation density of nuclei for increasing temperature can be explained by the increase in capture probability of a supercritical nucleus relative to the nucleation rate due to the increase in the carbon adatom mobility (at the low temperature regime) or desorption rate (at the high temperature regime), reducing the probability of further nucleation. Furthermore, reducing the rate of hydrocarbon decomposition by lowering the methane partial pressure (P_{CH_4}) can also decrease the density of the nuclei in which the effect is expected to be more significant at high temperatures.

More details on how eqs 1 and 2 were obtained are given in the Supporting Information, page S7.

So far we have modeled graphene nucleation on an ideal, smooth homogeneous surface. However, the polycrystalline Cu foil substrate exhibits various degrees of surface roughness, grain boundary grooves, and stepped terraces that may play an important role in determining the density and shape of the nuclei, and therefore the final density of grain boundaries of the polycrystalline graphene. Different surface morphologies can be induced by several types of features that are either extrinsic or intrinsic in nature. They include (1) rolling features and other large scale irregular dents and protrusions produced during foil manufacturing (Supporting Information, Figures S2 and S4a,b,d,e,), (2) grain boundary grooves evolving at higher temperatures due to the polycrystalline nature of the substrate[23,24] (Figure 4b), (3) phantom grain boundaries grooves formed during Cu grain growth[23,24] (Figure 4b), (4) step edges and kinks formed due to the misorientation of low-index crystal facets (Figure 4c), and (5) dislocations (Figure 4c).

On a bare Cu substrate we observed that after annealing at 1000 °C, the substrate rolling features become smooth as an expected effect of volume and surface self-diffusion of Cu,[25] but do not disappear completely (Figure 5b,e). Further, grain boundary grooves are naturally formed by Cu self-diffusion at high temperature and also phantom grain boundaries, a characteristic signature of boundary migration,[23] are visible on the transferred graphene film on SiO_2 (Figure 4b). We observe that these features can significantly affect graphene nucleation and growth. Preferential nucleation on top of the rolling marks in comparison with flat Cu area is observed as well as preferential growth of multilayer graphene at the grain boundaries and step edges/terraces of the grooves (Figure 4b). This is the experimental demonstration that step edges can act as energetically favorable sites for nucleation with lower size of critical nucleus and/or lower energy barrier for monomer attachment. Theoretical simulations[26] have recently predicted that lower size of critical nucleus is likely to occur at the metal step edges, although an experimental confirmation is still needed.

The lower energy barrier for carbon adsorption at step edges has been clearly demonstrated by monitoring *in situ* the evolution of carbon impurities at the single crystal Cu surface during cleaning of the surface by Ar^+ sputtering and annealing at about 950 °C. Through low energy electron microscope (LEEM) (Figure 4c) and X-ray photoemission electron microscopy (XPEEM) (Figure 4d), we could observe the segregation of residual carbon species (Supporting Information, Figure S4) and their preferential distribution along the Cu step edges and dislocations after several cycles of cleaning (Figure 4c,d). In Figure 4d, the C 1s core level intensity distribution across the surface reveals a higher concentration of carbon at the step edges in comparison to the flat areas. The C 1s binding energy (Figure 4e) is observed at 285.3 eV with fwhm of 1.4 eV. This indicates the presence of a complex mixture of sp^2/sp^3 carbon species with the possible presence of hydrogenated bonds.[27] Step−edges (location A) with variable carbon amount can be identified as well as carbon accumulation at the crystal dislocation (location B).

From the morphological and chemical characterization of the same region, it emerges that the dangling bonds at the Cu(100) step edges preferentially anchor carbon impurities that are probably from the manufacturing and handling process despite the fact that Cu at the surface is entirely reduced to its metallic state. However, we should also consider that these carbon impurities might be present also on the Cu foils annealed at 1000 °C in H_2. Indeed, *ex-situ* XPS has proven the presence of carbon impurities on the Cu foil after the surface preparation procedure while the Cu is completely reduced (Supporting Information, Figure S3). Therefore, we should consider that this residual carbon might perturb growth and contribute to the formation of multilayer graphene at the Cu step edges.

It is difficult to decouple the roles of temperature and surface morphology in imparting the density of nuclei as the latter evolves during annealing. Thus, we also compared nucleation and growth on as-received, annealed, and electropolished Cu substrates where no rough rolling features are present with surface roughness <3 nm (Figure 5c,f). In Figure 5g,h,i, we can see dissimilar nucleus densities and spatial distributions on the two surfaces after growth at 750 °C. On the unpolished sample (Figure 5g,h), graphene appears to preferentially nucleate along the rolling features

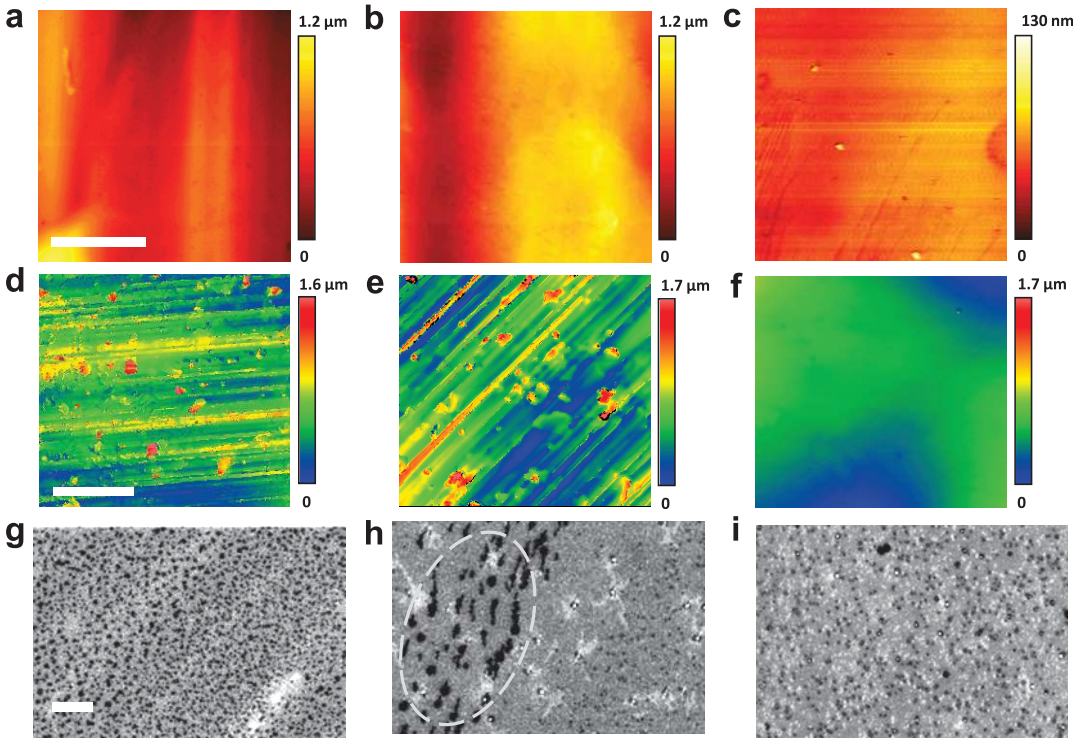

Figure 5. Effects of different Cu morphologies are compared in order to understand the preferential nucleation sites. (a, b, c) Surface profiles imaged by AFM (scale bar: 5 μm), (d, e, f) optical interferometry (scale bar: 100 μm), and (g, h, i) SEM (scale bar: 1 μm) performed on graphene/Cu samples produced at different polishing and annealing conditions. (a, d, g) Unpolished Cu substrate with annealing temperature of 750 °C and growth temperature of 750 °C; (b, e, h) unpolished Cu substrate with annealing temperature of 1000 °C and growth temperature of 750 °C. The dashed circle in panel h indicates a region of preferential nucleation on the rough area of Cu surface. (c, f, i) Electro-polished Cu substrate with annealing temperature of 1000 °C and growth temperature of 750 °C. Roughness measurement by AFM has yielded 18, 8, and 3 nm (rms) for samples a, b, and c, respectively.

evidenced by the higher density of nuclei in comparison with the lower density of nuclei away from the rolling features. While on the electropolished Cu substrates (Figure 5i), the density of nuclei was homogeneous over the whole surface. Contrary to the previous experimental finding,[6] the overall density of nuclei was actually higher for the electropolished sample. This is possibly due to the higher degree of supersaturation required for nucleation in the smoother surface resulting in larger $|c_{nuc} - c_{eq}|$. This could also explain the shorter time needed to reach full coverage on the polished sample (Supporting Information, Figure S5). However, electropolishing has some drawbacks as our observations suggest pitting of the Cu surface during the process could result in large defects in the graphene film (Figure S5b).

In addition, we can observe that the nucleus density on the smoother region of the as-received foil (Figure 5h) which contains the corrugated regions of alternating degree of surface roughness arising from the rolling features, is significantly lower (2 μm^{-2}) than the average density in the electropolished samples (11 μm^{-2}), which is uniformly flat. This is because the lower supersaturation carbon concentration is needed to nucleate graphene in the rough regions where the carbon-adatom species are less mobile, in comparison to a flat surface. As the nucleation occurs on the rough region first, the capture of carbon adatoms by the nuclei in the rough region will further reduce the likelihood of nucleation of the smooth region within the range of the nucleation exclusion zone that depends on the surface diffusion length of carbon adatom.[28] Therefore, under the same conditions of temperature and pressure, the resulting graphene nuclei density will be lower in the smoother regions of an alternating rough/smooth surface than the average density found on a uniformly flat, polished surface. In the light of this, we can conclude that the lowest nucleation density occurs not on a continuously smooth Cu surface, but on smooth regions of an alternating rough/smooth surface.

The graphene growth is a thermally activated process with a barrier energy of 2.6 $\pm$ 0.5 eV, as extracted from the Arrhenius plot given in Figure 6a and Supporting Information, Figure S6. This calculated activation energy is the same for all growth times and temperature ranges where significant coalescence does not occur, indicating that the energy is not nucleus-size-dependent and that the whole growth can be described by a single mechanism. To define the activation energy path, we need to consider the fundamental processes that can lead to the growth of a

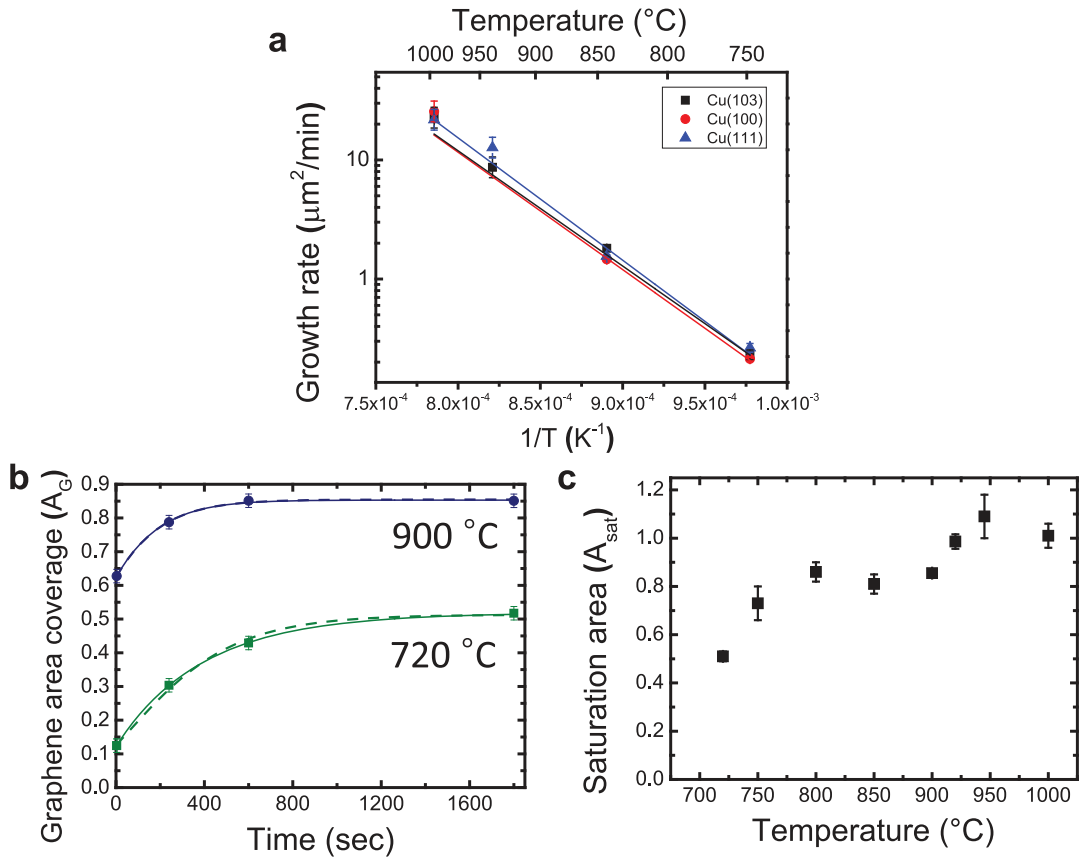

Figure 6. Analysis of graphene growth behavior. (a) Semilogarithmic plot of graphene nucleus growth rate *vs* 1/*T* for the three main crystal orientations of the substrate [Cu(103), Cu(100), and Cu(111)]. The growth rate for each data point was obtained by calculating the mean nucleus area per growth time, assuming that the growth is linear for a short growth time. The activation energy for the growth of a nucleus is extracted from the slope of the linear fit. (b) Graphene area coverage *vs* time behavior comparing the curve fits from eqs 4 (dashed line) and 6 (solid line). (c) Variation of saturation graphene area (A_{sat}) with temperature.

nucleus: (1) dissociative adsorption of CH_4 on the catalyst surface, (2) surface diffusion of the carbon species, and (3) enlargement of the graphene nuclei through attachment of carbon species. As the processes are sequential, the activation energy corresponds to the rate-limiting step with the largest energy barrier. We can first rule out step (1) as the possible rate-limiting step since the dissociative adsorption of CH_4 to carbon adatom on Cu(111) has an estimated barrier of 1.7−1.9 eV.[20−22] These values are significantly lower than the observed activation energy for the graphene growth, thus we can exclude this as the rate-limiting step. Also the low energy barrier for process 2 has been estimated to be as low as 0.07 eV for a monomer and 0.6 eV for a dimer.[17,19] Therefore, on the basis of our analysis, the growth limiting factor appears to be the attachment of carbon at the growing front of a nucleus. This finding is consistent with previous work on graphene growth on Cu(100) under UHV conditions.[29]

The activation energy of carbon attachment in the graphene epitaxial growth on Ru(0001)[13,14] has been experimentally calculated to be 2 eV which is slightly lower than the energy that we found for graphene on Cu (2.6 eV). This suggests that metals with high carbon affinity may catalyze the formation of C sp^2 carbon more efficiently than Cu or other noble metals (Au and Ag).[30]

To determine whether the Cu grain orientation may affect the growth activation energy, we have specifically measured growth rates of graphene nuclei on three main crystalline orientations [Cu(111), Cu(100), and Cu(103)] of the polycrystalline Cu. No significant differences in the activation energies (Figure 6a) have been found which leads us to confirm that filled symmetric 3d-electron shells of Cu are very stable, inducing Cu to form only soft bonds with carbon *via* charge transfer from the p electrons in the sp^2 hybridized carbon to the empty 4s states of Cu.[30] The energy involved in these bonds must be much lower than the activation energy for the graphene growth. A recent study of graphene grown on Cu(111) reports that growth rate is limited by diffusion and not attachment at the edges.[31] This is possibly due to the fact that the carbon concentration in that study is very low so that the growth is likely limited by the arrival rate of carbon adatoms rather than the attachment.

A simple model of edge controlled kinetics can be used to describe the growth of graphene islands on the

Cu surface. Considering that graphene arises from the crystallization of a supersaturated fraction of carbon adatom concentration ($c_{nuc} - c_{eq}$) according to our description, we could write the rate of graphene growth as the difference between carbon atoms attaching to the graphene edges and those leaving per unit time:

$$\frac{dA_G}{dt} = k_1 c_{cu}\sqrt{A_G} - k_2\sqrt{A_G} \quad (3)$$

where $k_1 c_{cu} {A_G}^{1/2}$ are the atoms arriving, that are proportional to the concentration of adsorbed atoms on the graphene-free Cu surface and to the perimeter of the graphene island (${A_G}^{1/2}$) and $k_2 {A_G}^{1/2}$ is the rate of atoms leaving. All the magnitudes are per unit of area of substrate. Because in our model, the adsorption and desorption rate are balanced once supersaturation is reached, the total number of carbon atoms adsorbed per unit area during graphene nucleation and growth remains constant (c_{nuc}) such that we can write:

$$c_{cu} = c_{nuc} - c_G \quad (4)$$

where c_G is equal to the number of atoms in graphene. If ρ_G is the atomic area density of graphene, 0.382 Å^{-2}:

$$c_G = A_G \rho_G \quad (5)$$

Solving eq 3 we can write the evolution of the graphene area coverage as

$$A_G = A_{sat}\left(\frac{\exp(k_1\rho_G\sqrt{A_{sat}}(t - t_0)) + 1}{\exp(k_1\rho_G\sqrt{A_{sat}}(t - t_0)) - 1}\right)^2 \quad (6)$$

where

$$A_{sat} = \frac{c_{nuc} - c_{eq}}{\rho_G} \quad (7)$$

is the saturation area of graphene for which $dA_G/dt = 0$ as $t \Longrightarrow \infty$, $c_{cu} \Longrightarrow c_{eq} = k_2/k_1$; t_0 is the nucleation time (time required for observable nuclei to form before significant growth). Equation 6 fits well the experimental data (Figure 6b). This simple model assumes instantaneous nucleation (which seems to be consistent with the observations) and although it does not account for the coalescence of the graphene islands the fitting supports two of the key observations of our analysis: carbon attachment is the rate limiting step and the amount of supersaturation, $|c_{nuc} - c_{eq}|$, determines the final extent of coverage.

This analysis suggests that we can describe the formation of graphene as the two-dimensional "crystallization" of the carbon layer adsorbed on the Cu surface. In this case, the overall behavior from the early stage of nucleation to the later stage of graphene growth with coalescence and area saturation could also be described in a single step using the theoretical framework of the JMAK model. We can fit our data to an exponential curve using a modified JMAK equation to account for the saturation area (A_{sat})[32] (Figure 6b):

$$A_G = A_{sat}(1 - \exp(k(t - t_0)^n)) \quad (8)$$

where k is the rate constant and n is called the Avrami exponent which reflects dimensionality of the system and time-dependent rates of nucleation and growth. Under the JMAK model, n is expected to be defined by the following equation:[30]

$$n = b + pm \quad (9)$$

where the exact values of b, p, and m depend on the dimensionality of the growth and nucleation and growth rates with respect to time (Supporting Information, Table S1). An average of $n = 1.1 \pm 0.5$ is obtained for our experimental data. Although the large error for n possibly arises from nonhomogeneous nucleation and anisotropic growth rates on the rough, faceted Cu foil surface that can affect the value of the Avrami exponent, this value appears to be consistent with our experimental observations that imply instant nucleation ($b \approx 0$) and nonlinear 2D, attachment-controlled growth ($p < 1$, $m = 2$).

Having established this, we can now predict whether a given growth condition would produce a continuous or discontinuous graphene film by the difference between the supersaturation carbon level needed to nucleate graphene and the equilibrium level adsorbed on the Cu surface, $|c_{nuc} - c_{eq}|$, such that the final area fraction of graphene can be described by eq 7. Note that this assumes that the amount of carbon above the equilibrium level at nucleation is the only source for the formation of graphene, and no additional decomposition of methane occurs above the equilibrium level after the nucleation. If $|c_{nuc} - c_{eq}|/\rho_G > 1$, complete coverage with a continuous graphene film will result.

Figure 6c shows the dependence of A_{sat} on the growth temperature. The increasing trend of A_{sat} with increasing growth temperature below 1000 °C is in accordance with the prediction that the amount of excess carbon increases exponentially with temperature based on the experimental measurement of the sticking coefficient of methane on Cu.[33] The similar trend for larger c_{nuc} and c_{eq} at higher temperature has also been observed for the graphene growth in the Ru system.[13] Furthermore, this also gives the lower limit of c_{nuc} to be $\rho_G = 3.82 \times 10^{-15}$ cm^{-2} for the complete monolayer growth. Thus, by adjusting the growth conditions, it is possible to obtain graphene of various coverage and nucleus densities. An interesting case is where $|c_{nuc} - c_{eq}|/\rho_G \gg 1$ and more carbon species are present at the surface than the amount needed to form a continuous monolayer of graphene. We expect that either carbon adatoms will desorb at the surface of graphene or lead to the formation of multilayer graphene or even amorphous carbon at high excess as reported in many of the empirical studies.[4−7,34,35] Therefore a critical aspect of graphene CVD is the

control of $|c_{nuc} - c_{eq}|$ by selecting the right experimental conditions (atmosphere, temperature, substrate chemistry, and topography, *etc.*). Additional experiments to determine adatom carbon concentration at the prenucleation stages are currently pursued.

CONCLUSION

In summary, our analysis shows that graphene arises from the crystallization of a supersaturated fraction of carbon-adatom species and that its nucleation density is the result of competition between the rates of nucleus growth by adatom capture, surface diffusion of carbon species, and desorption of carbon adatoms. As the energetics of these phenomena varies with temperature, the nucleation activation energies can change significantly with temperature, thus defining two nucleation density regimes: one controlled by carbon adatom species capture at low temperatures (<870 °C) and the other, controlled by desorption at high temperatures (>870 °C). In all cases, a pivotal role is played by the substrate roughness. Interestingly, on the basis of our model and experimental observation, the graphene nucleus density can be lower in the flat regions of an alternating rough/flat surface than the average density found on a uniformly flat substrate. On the other hand, the graphene growth can be uniquely described by the carbon attachment to the graphene edges as the rate-limiting step with activation energy of 2.6 eV and did not depend on the crystal orientation of the substrate. Control over the difference between the supersaturation carbon concentration, which is needed to nucleate graphene, and the equilibrium concentration of adsorbed carbon species on the Cu surface enables production of a continuous, pinhole-free graphene film.

Our analysis provides the physical model that can guide the synthesis of single crystal graphene films by carefully engineering the substrate surface and selecting growth conditions. Strategies to activate the carbon feed-stock and to engineer variably active step surfaces could be considered in order to lower the growth activation energy while maintaining a low level of nucleation density.

METHODS

The Chemical Vapor Deposition of Graphene on Cu. The chemical vapor deposition was performed in a low pressure, hot wall, tube furnace system. The 25 μm thick Cu foil was immersed in acetic acid at room temperature for 15 min before being loaded into the furnace to remove the surface oxides. Immediately after the acetic acid treatment, the foil was placed inside a quartz tube (3.6 cm in diameter and 1 m in length) that was loaded into the horizontal cylindrical furnace (heating zone length, 47 cm). The quartz tube was evacuated by a rotary pump with a base pressure of 1×10^{-3} mbar, and 100 sccm of Ar was introduced into the chamber for 30 min to replace air before heating the furnace to annealing/growth temperature of 720−1000 °C (Supporting Information, Figure S1). During the heating qstage, the flow rate of H_2 gas was 5 sccm. After annealing with the same H_2 flow rate for 30 min, CH_4 was introduced to the furnace at the flow rate of 0.5 sccm during the growth stage (growth pressure = 4.1 mbar). After the growth time of 1 s (flash exposure) to 30 min, CH_4 was shut off, and the furnace was allowed to cool down naturally with a hydrogen flow of 5 sccm.

Transfer of Graphene on SiO_2. Initially, poly(methyl methacrylate) (PMMA) dissolved in anisole (MicroChem) was spin-coated on the as-grown graphene film on Cu foil. After which the Cu was etched in 3.5 g of $FeCl_3$ (Sigma Aldrich) dissolved in DI water (100 mL) and HCl (10 mL), and free-standing PMMA/graphene film floating on the water bath was obtained. Several washing cycles in DI water were necessary to eliminate residual of $FeCl_3$. The freestanding graphene/PMMA membrane was transferred onto SiO_2/Si substrates for further characterization. Final etching of the PMMA was obtained in an acetone bath at 55 °C for 30 min.

Electropolishing of Cu Foil. One side of Cu foil was coated with a polymer and immersed in DI water and phosphoric acid solution (1:2 volume ratio). Stainless steel tweezers were used to make electrical contact with Cu foil used as the anode and the stainless steel beaker was used as cathode. A voltage of 1.5−2 V was applied on the foil for 30 s. After the electropolishing, the foil was rinsed in water and cleaned in ultrasonic bath of acetone and ethanol.

Surface Profile Measurements. The surface topography was characterized by atomic force microscopy (Ambios Technology) in contact mode and ZYGO optical interferometer (NewView 200, System: OMP-0407C, Software: MetroPro) in ambient conditions.

Conflict of Interest: The authors declare no competing financial interest.

Acknowledgment. This project was financially supported by the Leverhume Trust and NSERC, Canada. We thank S. Eslava for optical interferometric measurements and A. Locatelli and T. O. Menteş for carrying out LEEM and XPEEM experiments (Nanospectroscopy beamline, Elettra Synchrotron Laboratory, Italy) and their valuable feedback.

Supporting Information Available: Additional figures and data as described in the text. This material is available free of charge *via* the Internet at http://pubs.acs.org.

REFERENCES AND NOTES

1. Li, X.; Cai, W.; An, J.; Kim, S.; Nah, J.; Yang, D.; Piner, R.; Velamakanni, A.; Jung, I.; Tutuc, E.; *et al.* Large-Area Synthesis of High-Quality and Uniform Graphene Films on Copper Foils. *Science* **2009**, *324*, 1312–1314.
2. Huang, P. Y.; Ruiz-Vargas, C. S.; van der Zande, A. M.; Whitney, W. S.; Levendorf, M. P.; Kevek, J. W.; Garg, S.; Alden, J. S.; Hustedt, C. J.; Zhu, Y.; *et al.* Grains and Grain Boundaries in Single-Layer Graphene Atomic Patchwork Quilts. *Nature* **2011**, *469*, 389–392.
3. Ivan, V.; Sergei, S.; Ilia, I.; Pasquale, F. F.; Sheng, D.; Harry, M.; Miaofang, C.; Dale, H.; Panos, D.; Nickolay, V. L. Electrical and Thermal Conductivity of Low Temperature CVD Graphene: The Effect of Disorder. *Nanotechnology* **2011**, *22*, 275716.
4. Li, X.; Magnuson, C. W.; Venugopal, A.; Tromp, R. M.; Hannon, J. B.; Vogel, E. M.; Colombo, L.; Ruoff, R. S. Large-Area Graphene Single Crystals Grown by Low-Pressure Chemical Vapor Deposition of Methane on Copper. *J. Am. Chem. Soc.* **2011**, *133*, 2816.
5. Vlassiouk, I.; Regmi, M.; Fulvio, P.; Dai, S.; Datskos, P.; Eres, G.; Smirnov, S. Role of Hydrogen in Chemical Vapor

Deposition Growth of Large Single-Crystal Graphene. *ACS Nano* **2011**, *5*, 6069–6076.
6. Luo, Z.; Lu, Y.; Singer, D. W.; Berck, M. E.; Somers, L. A.; Goldsmith, B. R.; Johnson, A. T. C. Effect of Substrate Roughness and Feedstock Concentration on Growth of Wafer-Scale Graphene at Atmospheric Pressure. *Chem. Mater.* **2011**, *23*, 1441–1447.
7. Bhaviripudi, S.; Jia, X.; Dresselhaus, M. S.; Kong, J. Role of Kinetic Factors in Chemical Vapor Deposition Synthesis of Uniform Large Area Graphene Using Copper Catalyst. *Nano Lett.* **2010**, *10*, 4128–4133.
8. Zhao, L.; Rim, K. T.; Zhou, H.; He, R.; Heinz, T. F.; Pinczuk, A.; Flynn, G. W.; Pasupathy, A. N. Influence of Copper Crystal Surface on the CVD Growth of Large Area Monolayer Graphene. *Solid State Commun.* **2011**, *151*, 509–513.
9. Robinson, V. N. E.; Robins, J. L. Nucleation Kinetics of Gold Deposited onto UHV Cleaved Surfaces of NaCl and KBr. *Thin Solid Films* **1974**, *20*, 155–175.
10. Avrami, M. Kinetics of Phase Change. I General Theory. *J. Chem. Phys.* **1939**, *7*, 1103–1112.
11. Kolmogorov, A. N. Statistical Theory of Crystallization of Metals. *Izv. Akad. Nauk SSSR, Ser. Fiz. Mat. Nauk.* **1937**, *3*, 355–360.
12. Johnson, W. A.; Mehl, R. F. Reaction Kinetics in Processes of Nucleation and Growth. *Trans. Am. Inst. Min., Metall. Pet. Eng.* **1939**, *135*, 416.
13. Loginova, E.; Norman, C. B.; Peter, J. F.; Kevin, F. M. Evidence for Graphene Growth by C Cluster Attachment. *New J. Phys.* **2008**, *10*, 093026.
14. Loginova, E.; Bartelt, N. C.; Feibelman, P. J.; McCarty, K. F. Factors Influencing Graphene Growth on Metal Surfaces. *New J. Phys.* **2009**, *11*, 063046.
15. Van Wesep, R. G.; Chen, H.; Zhu, W.; Zhang, Z. Communication: Stable Carbon Nanoarches in the Initial Stages of Epitaxial Growth of Graphene on Cu(111). *J. Chem. Phys.* **2011**, *134*, 171105–4.
16. Zhang, W.; Wu, P.; Li, Z.; Yang, J. First-Principles Thermodynamics of Graphene Growth on Cu Surfaces. *J. Phys. Chem. C* **2011**, *115*, 17782–17787.
17. Wu, P.; Zhang, W.; Li, Z.; Yang, J.; Hou, J. G. Communication: Coalescence of Carbon Atoms on Cu (111) Surface: Emergence of a Stable Bridging-Metal Structure Motif. *J. Chem. Phys.* **2010**, *133*, 071101–4.
18. Lewis, B.; Anderson, J. C. *Nucleation and Growth of Thin Films*; Academic Press Inc.: New York, 1978.
19. Yazyev, O. V.; Pasquarello, A. Effect of Metal Elements in Catalytic Growth of Carbon Nanotubes. *Phys. Rev. Lett.* **2008**, *100*, 156102.
20. Gajewski, G.; Pao, C.-W. *Ab Initio* Calculations of the Reaction Pathways for Methane Decomposition over the Cu (111) Surface. *J. Chem. Phys.* **2011**, *135*, 064707.
21. An, W.; Zeng, X. C.; Turner, C. H. First-Principles Study of Methane Dehydrogenation on a Bimetallic Cu/Ni(111) Surface. *J. Chem. Phys.* **2009**, *131*, 174702–11.
22. Au, C.-T.; Ng, C.-F.; Liao, M.-S. Methane Dissociation and Syngas Formation on Ru, Os, Rh, Ir, Pd, Pt, Cu, Ag, and Au: A Theoretical Study. *J. Catal.* **1999**, *185*, 12–22.
23. Mullins, W. W. Theory of Thermal Grooving. *J. Appl. Phys.* **1957**, *28*, 333–339.
24. Mullins, W. W.; Shewmon, P. G. The Kinetics of Grain Boundary Grooving in Copper. *Acta Metall.* **1959**, *7*, 163–170.
25. Hoehne, K.; Sizmann, R. Volume and Surface Self-diffusion Measurements on Copper by Thermal Surface Smoothing. *Phys. Status Solidi A* **1971**, *5*, 577–589.
26. Saadi, S.; Abild-Pedersen, F.; Helveg, S.; Sehested, J.; Hinnemann, B.; Appel, C. C.; Nørskov, J. K. On the Role of Metal Step-Edges in Graphene Growth. *J. Phys. Chem. C* **2010**, *114*, 11221–11227.
27. Díaz, J.; Paolicelli, G.; Ferrer, S.; Comin, F. Separation of the sp^3 and sp^2 Components in the C1s Photoemission Spectra of Amorphous Carbon Films. *Phys. Rev. B* **1996**, *54*, 8064–8069.
28. Markov, I.; Kashchiev, D. The Effect of Substrate Inhomogeneity on the Kinetics of Heterogeneous Nucleation from Vapours. *Thin Solid Films* **1973**, *15*, 181–189.
29. Wofford, J. M.; Nie, S.; McCarty, K. F.; Bartelt, N. C.; Dubon, O. D. Graphene Islands on Cu Foils: The Interplay between Shape, Orientation, and Defects. *Nano Lett.* **2010**, *10*, 4890–4896.
30. Earnshaw, A.; Harrington, T. J. *The Chemistry of the Transition Elements*; Clarendon Press: 1973.
31. Nie, S.; Wofford, J. M.; Bartelt, N. C.; Dubon, O. D.; McCarty, K. F. Origin of the Mosaicity in Graphene Grown on Cu(111). *Phys. Rev. B* **2011**, *84*, 155425.
32. Sharples, A., Introduction to Polymer Crystallization. In *Overall Kinetics of Crystallization*; Sharples, A., Ed.; Edward Arnold Ltd.: London, 1966; pp 44−59.
33. Alstrup, I.; Chorkendorff, I.; Ullmann, S. The Interaction of CH_4 at High Temperatures with Clean and Oxygen Precovered Cu(100). *Surf. Sci.* **1992**, *264*, 95–102.
34. Li, X.; Magnuson, C. W.; Venugopal, A.; An, J.; Suk, J. W.; Han, B.; Borysiak, M.; Cai, W.; Velamakanni, A.; Zhu, Y.; *et al*. Graphene Films with Large Domain Size by a Two-Step Chemical Vapor Deposition Process. *Nano Lett.* **2010**, *10*, 4328–4334.
35. Han, G. H.; Güneş, F.; Bae, J. J.; Kim, E. S.; Chae, S. J.; Shin, H.-J.; Choi, J.-Y.; Pribat, D.; Lee, Y. H. Influence of Copper Morphology in Forming Nucleation Seeds for Graphene Growth. *Nano Lett.* **2011**, *11*, 4144–4148.